



# C<sub>x</sub>N<sub>y</sub>: New Carbon Nitride Organic Photocatalysts

Nieves López-Salas\* and Josep Albero\*

Max Planck Institute of Colloids and Interfaces, Research Campus Golm, University of Potsdam, Potsdam, Germany

## OPEN ACCESS

### Edited by:

Ching-Hwa Ho,  
National Taiwan University of Science  
and Technology, Taiwan

### Reviewed by:

Asadollah Bafekry,  
Shahid Beheshti University, Iran  
Sumesh. CK,  
Charotar University of Science and  
Technology, India

### \*Correspondence:

José Albero  
joalsan6@upvnet.upv.es  
Nieves Lopez-Salas  
nieves.lopezsalas@mpikg.mpg.de

### Specialty section:

This article was submitted to  
Semiconducting Materials and  
Devices,  
a section of the journal  
Frontiers in Materials

Received: 07 September 2021

Accepted: 04 October 2021

Published: 01 December 2021

### Citation:

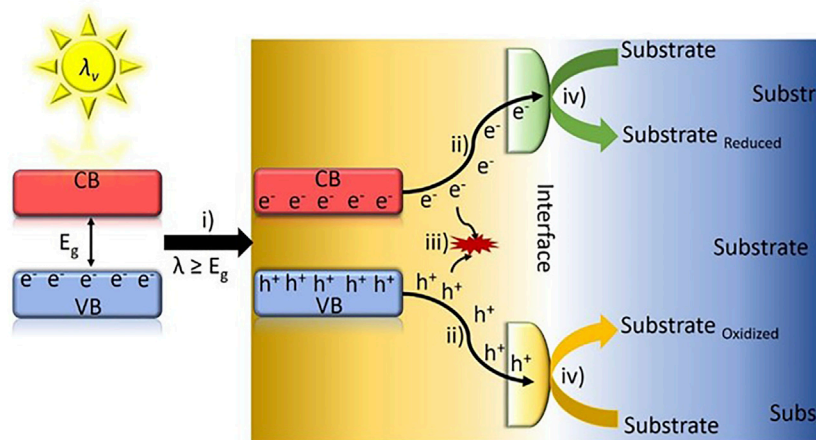
López-Salas N and Albero J (2021)  
C<sub>x</sub>N<sub>y</sub>: New Carbon Nitride  
Organic Photocatalysts.  
Front. Mater. 8:772200.  
doi: 10.3389/fmats.2021.772200

The search for metal-free and visible light-responsive materials for photocatalytic applications has attracted the interest of not only academics but also the industry in the last decades. Since graphitic carbon nitride (g-C<sub>3</sub>N<sub>4</sub>) was first reported as a metal-free photocatalyst, this has been widely investigated in different light-driven reactions. However, the high recombination rate, low electrical conductivity, and lack of photoresponse in most of the visible range have elicited the search for alternatives. In this regard, a broad family of carbon nitride (C<sub>x</sub>N<sub>y</sub>) materials was anticipated several decades ago. However, the attention of the researchers in these materials has just been awakened in the last years due to the recent success in the syntheses of some of these materials (i.e., C<sub>3</sub>N<sub>3</sub>, C<sub>2</sub>N, C<sub>3</sub>N, and C<sub>3</sub>N<sub>5</sub>, among others), together with theoretical simulations pointing at the excellent physico-chemical properties (i.e., crystalline structure and chemical morphology, electronic configuration and semiconducting nature, or high refractive index and hardness, among others) and optoelectronic applications of these materials. The performance of C<sub>x</sub>N<sub>y</sub>, beyond C<sub>3</sub>N<sub>4</sub>, has been barely evaluated in real applications, including energy conversion, storage, and adsorption technologies, and further work must be carried out, especially experimentally, in order to confirm the high expectations raised by simulations and theoretical calculations. Herein, we have summarized the scarce literature related to recent results reporting the synthetic routes, structures, and performance of these materials as photocatalysts. Moreover, the challenges and perspectives at the forefront of this field using C<sub>x</sub>N<sub>y</sub> materials are disclosed. We aim to stimulate the research of this new generation of C<sub>x</sub>N<sub>y</sub>-based photocatalysts, beyond C<sub>3</sub>N<sub>4</sub>, with improved photocatalytic efficiencies by harnessing the striking structural, electronic, and optical properties of this new family of materials.

**Keywords:** C<sub>x</sub>N<sub>y</sub>, carbon nitrides, C<sub>2</sub>N, C<sub>3</sub>N, C<sub>1</sub>N<sub>1</sub>, C<sub>3</sub>N<sub>5</sub>, photocatalysis

## INTRODUCTION

The conversion of inexhaustible and clean sunlight into chemicals and fuels by means of a photocatalyst has been pointed out as an appealing approach to mitigate the energy crisis as well as the environmental concerns caused by the massive consumption of fossil fuels. In a typical photocatalytic process, the photocatalyst, typically a semiconductor material, must absorb photons with energy equal or larger than that of its band gap. After light-harvesting, electrons (e<sup>-</sup>) in the valence band (VB) are promoted to the conduction band (CB), leaving a positive charge, named hole (h<sup>+</sup>), in the VB. The photo-generated electron-hole pairs must migrate to an interface between the semiconductor surface and the reaction media before undesirable charge recombination takes place.



**Scheme 1** | Schematic diagram of semiconductor photocatalytic reaction mechanism and the fundamental steps taking place. (i) Photo-induced electron  $e^-/h^+$  pairs, (ii) charge carriers migration to the semiconductor surface, (iii) charge recombination, and (iv) red/ox reactions.

Finally, the photo-generated electrons and holes at the interface are involved in red/ox reactions. **Scheme 1** presents the fundamental steps of the photocatalytic process.

A large variety of semiconductor photocatalysts, such as TiO<sub>2</sub>, ZnO, Fe<sub>2</sub>O<sub>3</sub>, BiVO<sub>4</sub>, SrTiO<sub>3</sub>, WO<sub>3</sub>, CdS, MoS<sub>2</sub>, MOFs, etc., have been widely investigated in different photocatalytic applications such as water splitting, artificial photosynthesis, N<sub>2</sub> fixation, organic transformations, and pollutant degradation (Yang and Wang, 2018). Among them, TiO<sub>2</sub> has been the most widely studied photocatalyst since the seminal paper of Fujishima and Honda (1972). However, TiO<sub>2</sub> is a wide-band gap semiconductor (3.2 eV for anatase), and therefore, only photons from the UV region of the solar spectrum, which accounts for less than 4% of the total solar irradiation, can be involved in photocatalytic reactions, rendering low production rates. Other narrow-band gap semiconductors, such as Cu<sub>2</sub>O or Fe<sub>2</sub>O<sub>3</sub>, have shown large instability and/or suffering from high recombination rates (Zhou et al., 2016). Similarly, metal sulfides are also well known to decompose upon light irradiation (Iwashina et al., 2015; Ning and Lu, 2020). For these reasons, metal-free carbon-based semiconductor materials (doped graphenes, carbon nanotubes, carbon dots, carbon nitrides, etc.) have been recently proposed as good candidates in photocatalytic applications due to their robustness, large surface area, and optoelectronic properties, among others (Jin et al., 2018; Albero et al., 2019; Chu et al., 2020; Guo et al., 2020; Haiyan et al., 2020; Kandy, 2020; Mazzanti and Savateev, 2020; Reischauer and Pieber, 2021; Zou et al., 2021).

In this regard, the carbon nitride material family (C<sub>x</sub>N<sub>y</sub>) has attracted increasing interest in the last decades, and the number of both theoretical and experimental publications have grown exponentially in this field. Among them, the most widely studied so far has been the graphitic carbon nitride (g-C<sub>3</sub>N<sub>4</sub>), which was first reported in photocatalytic applications by Wang et al. (2009). This is a metal-free semiconductor material formed by the stacking of g-C<sub>3</sub>N<sub>4</sub> layers consisting of tri-s-triazine units linked by amino groups. g-C<sub>3</sub>N<sub>4</sub> can be prepared by thermal

condensation of N-rich precursors, such as urea, thiourea, cyanamide, dicyanamide, and melamine, among others (Lakhi et al., 2017). Moreover, g-C<sub>3</sub>N<sub>4</sub> has demonstrated suitable optoelectronic properties (2.7 eV band gap) as well as a high thermal, mechanical, and chemical stability. As a consequence, a wide variety of C<sub>3</sub>N<sub>4</sub>-based photocatalysts have been investigated to drive chemical reactions upon light irradiation (Wang L. et al., 2020), including H<sub>2</sub> evolution from water (Naseri et al., 2017), pollutants degradation (Ong et al., 2016), CO<sub>2</sub> reduction (Liu R. et al., 2020), and organic transformations, such as aromatic compounds oxidation, benzaldehyde and alcohol esterifications, oxidative cleavage of C–C bonds and allylic oxidations, among others (Wen et al., 2017). Nevertheless, the performance of C<sub>3</sub>N<sub>4</sub> in photocatalytic applications is still limited since this is highly dependent on the crystal structure, porosity, charge transport, and the limited light harvesting in the visible (Vis) and near-infrared (NIR) regions. For that reason, crystalline carbon nitrides with different stoichiometry than that of C<sub>3</sub>N<sub>4</sub> have recently emerged exhibiting very promising properties for optoelectronic applications (Tan et al., 2021).

Theoretical calculations have predicted different C<sub>x</sub>N<sub>y</sub> crystalline structures, beyond C<sub>3</sub>N<sub>4</sub>, with striking properties since 1989. The mechanical, optical, electronic, and structural properties of this new family of materials have been anticipated by DFT and first-principles calculations. Moreover, theoretical efforts are also being invested in the theoretical design of the materials (Kou et al., 2020). The wide range of compositional possibilities within these materials (CN, C<sub>2</sub>N, C<sub>3</sub>N, and C<sub>3</sub>N<sub>5</sub>, etc.), giving rise to the fine tune of their properties, have motivated not only theoretical but also experimental researchers to explore the performance of these materials in different fields, including electronics, sensing, mechanical, adsorbents, catalysis, photocatalysis, electrocatalysis and energy storage, among others (Tan et al., 2021).

C<sub>x</sub>N<sub>y</sub> materials have already shown great potential in energy storage and electronic applications due to their semiconducting

properties (Xu et al., 2017; Yang et al., 2017; Bafekry et al., 2019). However, the use of C<sub>x</sub>N<sub>y</sub> materials beyond g-C<sub>3</sub>N<sub>4</sub> in photocatalysis is in its infancy, and further work must be carried out, especially experimentally, in order to confirm the high expectations raised by simulations and theoretical calculations. In this review, we aim to overview the scarce experimental and theoretical reports in the field of photocatalysis using novel C<sub>x</sub>N<sub>y</sub> materials, except g-C<sub>3</sub>N<sub>4</sub> which has been widely reviewed elsewhere (Ong et al., 2016; Wen et al., 2017; Fang and Wang, 2018; Savateev et al., 2018; Nasir et al., 2019). We have paid special emphasis on the synthetic procedures and the crystalline structures of the obtained materials that have given rise to very promising performances as photocatalysts. Finally, we will look for the best candidates in this area based on the available experimental results and theoretical calculations, which could give rise to the next generation of metal-free carbon-based materials in photocatalysis.

## C<sub>3</sub>N<sub>5</sub>

The motivation in the preparation of nitrogen-rich carbon nitrides arise from the large band gap that the undoped g-C<sub>3</sub>N<sub>4</sub> exhibits (2.7 eV,  $\lambda < 450$  nm), which limits the application of this semiconductor in the photocatalytic field. A straightforward way to reduce its band gap goes through the addition of more N atoms in the carbon nitride framework. In this regard, Mane et al. reported in 2017, for the first time, a synthetic procedure, which enabled the formation of a well-ordered 3D porous carbon nitride with stoichiometry C<sub>3</sub>N<sub>5</sub>, exhibiting a band gap energy of 2.2 eV (Mane et al., 2017). This C<sub>3</sub>N<sub>5</sub> semiconductor material was prepared using a single molecular precursor with a high nitrogen content (3-amino-1,2,4-triazole) by means of a hard templating approach through precursor self-condensation inside the confined mesopores of KIT-6 silica at 500°C in Ar atmosphere. After carbonization, the silica template was dissolved in HF, and the obtained C<sub>3</sub>N<sub>5</sub> was filtered and washed with EtOH. The sample exhibited ordered mesopores with a pore size of 3.42 nm and a specific surface area of 296.7 m<sup>2</sup>/g.

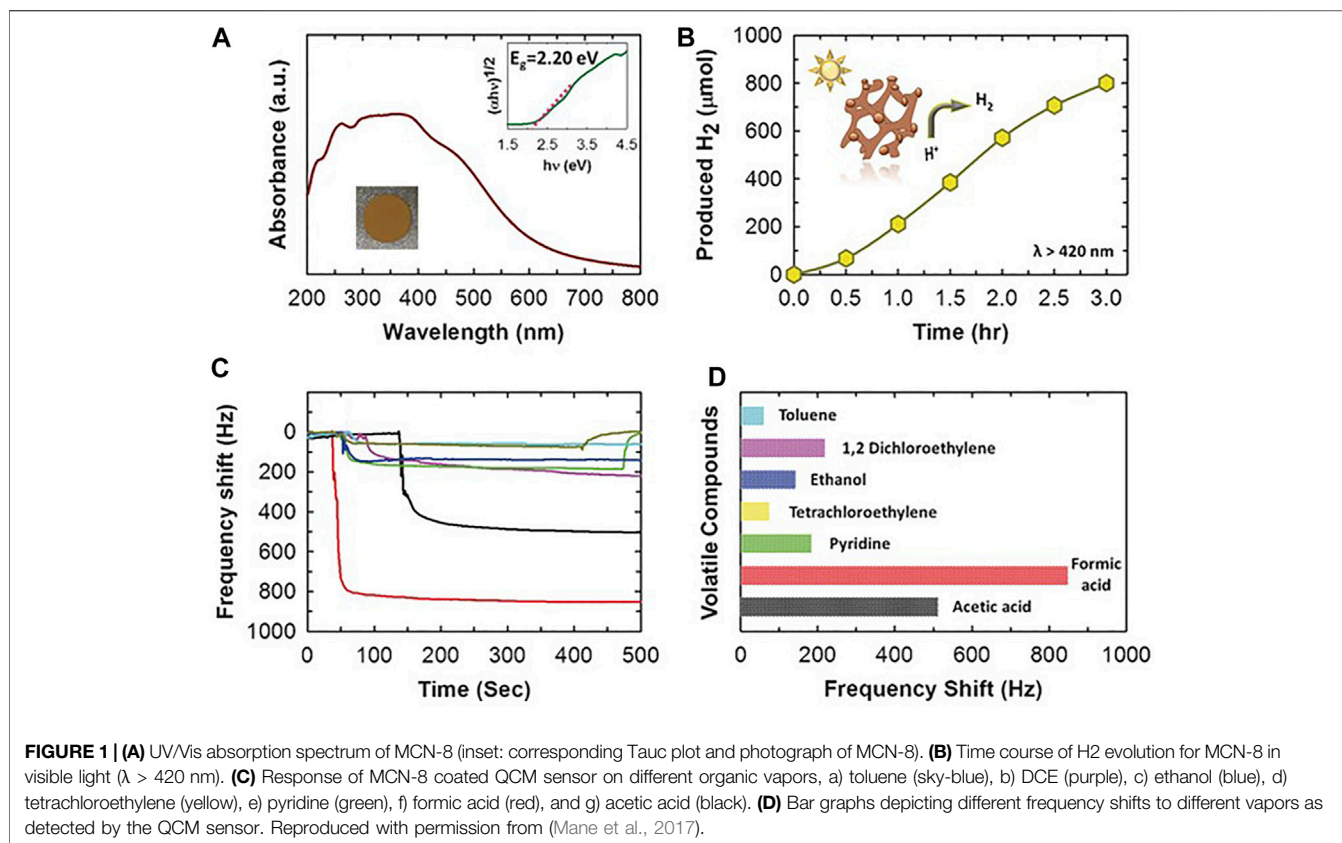
Synchrotron-based near-edge XRD fine structure (NEXAFS) showed three peaks characteristic of the carbon structure, very similar to the KIT-6 mesoporous silica, indicating that the obtained structure is very similar to that of the template. The as-prepared C<sub>3</sub>N<sub>5</sub> presented a broad absorption band covering the whole UV-Vis spectrum (Figure 1), and its performance in photocatalytic H<sub>2</sub> evolution was investigated. Pt nanoparticles were photo-deposited on the semiconductor surface, and Pt-C<sub>3</sub>N<sub>5</sub> aqueous dispersions (1 mg/ml) containing triethanolamine (10 vol.%) were irradiated under the outcome of a 300-W Xe lamp filtered with a long-pass cutoff filter ( $\lambda \geq 420$  nm). The photocatalytic H<sub>2</sub> production under these conditions was of 801  $\mu$ mol after 3 h irradiation. The H<sub>2</sub> evolution rate of C<sub>3</sub>N<sub>5</sub> was found much higher than that of C<sub>3</sub>N<sub>4</sub> reported in the literature under similar conditions. It was determined that the reduced band gap not only enhanced the light harvesting of a large portion of the visible region of the solar

spectrum but also provided more favorable thermodynamics for H<sup>+</sup> reduction.

One of the most applied methods was developed by Zhang, Yan, and co-workers. They prepared a rod-like C<sub>3</sub>N<sub>5</sub> material with a length up to 1–6  $\mu$ m and a diameter of 100–500 nm through a KBr-guided approach using 3-amino-1,2,4-triazole as C<sub>3</sub>N<sub>5</sub> precursor and KBr acting as guide (Wang et al., 2019). In this method, an aqueous solution containing KBr and the C<sub>3</sub>N<sub>5</sub> precursor was heated at 80°C, and the water solvent was allowed to gently evaporate until the KBr crystals grew covered by the molecular precursor. The obtained solid was annealed at 500°C in air conditions. Finally, C<sub>3</sub>N<sub>5</sub> was easily recovered by water washing. Opposite to the previous method, where HF was used to remove the silica template, these approach is more environmentally friendly and easy. However, the KBr-guided approach promoted rod-like shape C<sub>3</sub>N<sub>5</sub> (Figure 2), exhibiting a 1.90 eV band gap. XRD patterns showed a diffraction peak at 13.4° attributed to the 100 facets, indicating the in-plane structural ordering of the obtained C<sub>3</sub>N<sub>5</sub>. In this report, the photocatalytic activity toward organic pollutant degradation using the model contaminant methylene blue (MB) was studied dispersing the C<sub>3</sub>N<sub>5</sub>-based photocatalyst (1 mg/ml) in an MB solution (20 mg/ml) and irradiated under visible light ( $\lambda \geq 420$  nm) with a 50 W-halogen tungsten lamp. For comparison purposes, pristine g-C<sub>3</sub>N<sub>5</sub> was prepared, and the photocatalytic degradation of MB was studied too. It was demonstrated that the photocatalytic degradation ratios of pristine g-C<sub>3</sub>N<sub>5</sub> and rod-like C<sub>3</sub>N<sub>5</sub> reached 10% and 98% within 120 min, respectively. The authors ascribed the improved photocatalytic activity of the rod-like C<sub>3</sub>N<sub>5</sub> to the higher surface area and smaller band gap than that of the pristine g-C<sub>3</sub>N<sub>5</sub> (2.05 eV). Despite no comparison of the photocatalytic activity with other g-C<sub>3</sub>N<sub>4</sub> has been provided, the reduced band gap that this material presents allows much broader photo-response in the visible range of the solar spectrum than any undoped g-C<sub>3</sub>N<sub>4</sub>.

In a similar approach, Jin et al. reported the synthesis of g-C<sub>3</sub>N<sub>5</sub> following the previous approach based on the KBr-guided synthesis (Jin et al., 2020). The obtained g-C<sub>3</sub>N<sub>5</sub> was mixed with Zn<sub>0.5</sub>Cd<sub>0.5</sub>S, sonicated, and filtered with the aim to obtain composites exhibiting Z-scheme heterojunctions. After loading optimization (15 wt.% of g-C<sub>3</sub>N<sub>5</sub>), a photocatalytic H<sub>2</sub> production of 142.8 mmol/g·h using Na<sub>2</sub>S and Na<sub>2</sub>SO<sub>3</sub> as sacrificial electron donors, a 300-W Xe lamp (100 mW/cm<sup>2</sup>) as light source, and a quantum efficiency of 33.7% under 420-nm monochromatic light, was obtained. In this case, the authors reported that g-C<sub>3</sub>N<sub>5</sub> was used in the heterojunction instead of g-C<sub>3</sub>N<sub>4</sub> because of the smaller band gap and the antecedents in the literature supporting the better photocatalytic performance of g-C<sub>3</sub>N<sub>5</sub>. Similarly, Vadivel et al. reported identical synthetic approach to prepare AgCl-loaded g-C<sub>3</sub>N<sub>5</sub> composites for visible light photocatalytic pollutant degradation. In this work, Rhodamine B (RhB) was used as model pollutant, and the removal achieved 96% within 30-min efficiency under visible light irradiation with the output of a 300-W halogen lamp (Vadivel et al., 2020).

A variation of this method was reported by Zhang and collaborators (Li et al., 2020). In this, NaOH was used instead



of KBr with the aim to introduce N-vacancies in the g-C<sub>3</sub>N<sub>5</sub>. The N-vacancies promoted a redshift of the absorption edge due to a band gap narrowing from 2.08 up to 1.50 eV. XRD measurements of pristine g-C<sub>3</sub>N<sub>5</sub> and g-C<sub>3</sub>N<sub>5</sub> with N-vacancies (NV-g-C<sub>3</sub>N<sub>5</sub>) revealed a peak at 27.1° related to the 002 crystal planes of C<sub>3</sub>N<sub>5</sub>, while the 002 peak of NV-g-C<sub>3</sub>N<sub>5</sub> was shifted to a higher angle due to the repulsion between the electron-rich conjugated C<sub>3</sub>N<sub>5</sub> layers. Besides, the lower intensity of the 002 peak suggests that the CN framework is distorted, and as consequence, the ordered structure of g-C<sub>3</sub>N<sub>5</sub> is partially lost in NV-g-C<sub>3</sub>N<sub>5</sub>. The as-prepared NV-g-C<sub>3</sub>N<sub>5</sub> formed a heterojunction with BiOBr, and the composite material was tested as photocathode for nitrogen reduction. Thus, NV-g-C<sub>3</sub>N<sub>5</sub>/BiOBr was deposited on FTO and used as a working electrode. The photoelectrochemical nitrogen reduction was carried out under a Sun-simulated light with a cut off filter ( $\lambda \geq 420$  nm) in a three-electrode H-type cell with a proton exchange membrane, a saturated Ag/AgCl (sat. KCl) reference electrode, and a Pt sheet as a counter electrode in HCl + Na<sub>2</sub>SO<sub>4</sub> electrolyte. Under these conditions, a maximum NH<sub>3</sub> yield rate and Faraday efficiency of 29.4  $\mu\text{g}/\text{h}\cdot\text{mg}$  and 11%, respectively, at  $-0.2$  V were obtained. The authors concluded that the N-vacancies were not only effective in narrowing the band gap, but also acting as catalytic sites for the activation and reduction of N<sub>2</sub>.

Alternatively, ultrathin C<sub>3</sub>N<sub>5</sub> nanosheets were prepared following a two-step method based on, first, a NH<sub>4</sub>Cl-guided approach to obtain bulk g-C<sub>3</sub>N<sub>5</sub> and subsequent protonation

process consisting in bulk g-C<sub>3</sub>N<sub>5</sub> treatment with HNO<sub>3</sub> and H<sub>2</sub>SO<sub>4</sub> mixtures under continuous stirring for 12 h (Liu T. et al., 2020). The XRD pattern before and after protonation with the acids remained the same, exhibiting a peak at 27.3° attributed to the inter-layer stacking of the conjugated C<sub>3</sub>N<sub>5</sub> framework. The obtained 2D g-C<sub>3</sub>N<sub>5</sub> nanosheets with a surface area of 38 m<sup>2</sup>/g exhibited photocatalytic activity toward MB photodegradation as well as H<sub>2</sub> evolution under visible light irradiation ( $\lambda \geq 400$  nm) with a 300-W Xe lamp.

In a very appealing approach, Zhu and co-workers prepared g-C<sub>3</sub>N<sub>5</sub>/TiO<sub>2</sub> heterojunctions following the Zhan and Yan protocol, but replacing KBr by TiO<sub>2</sub> (Zhang et al., 2021). In this case, the guiding-metal oxide was not removed after annealing at 500°C, and instead, this is part of the photocatalytic system. XRD pattern showed a peak at 27.2° attributed to the 002 plane, indicating the interlayer stacking characteristic of this material. The composite exhibited excellent photocatalytic activity in visible light driven ( $\lambda \geq 400$  nm) from a 300-W Xe lamp, with NO photooxidation under relative humidity of 15%. It is worth commenting that this composite photocatalyst presented high stability, and after six consecutive runs, the NO removal efficiency only showed 7% loss, from 67% to 60%.

A very different approach was reported by Kumar et al. by thermal deammoniation of 2,5,8-trihydrazino-s-heptazine (melem) (Kumar et al., 2019). In this, melem hydrazine was first synthesized by hydrothermal reaction between melem and

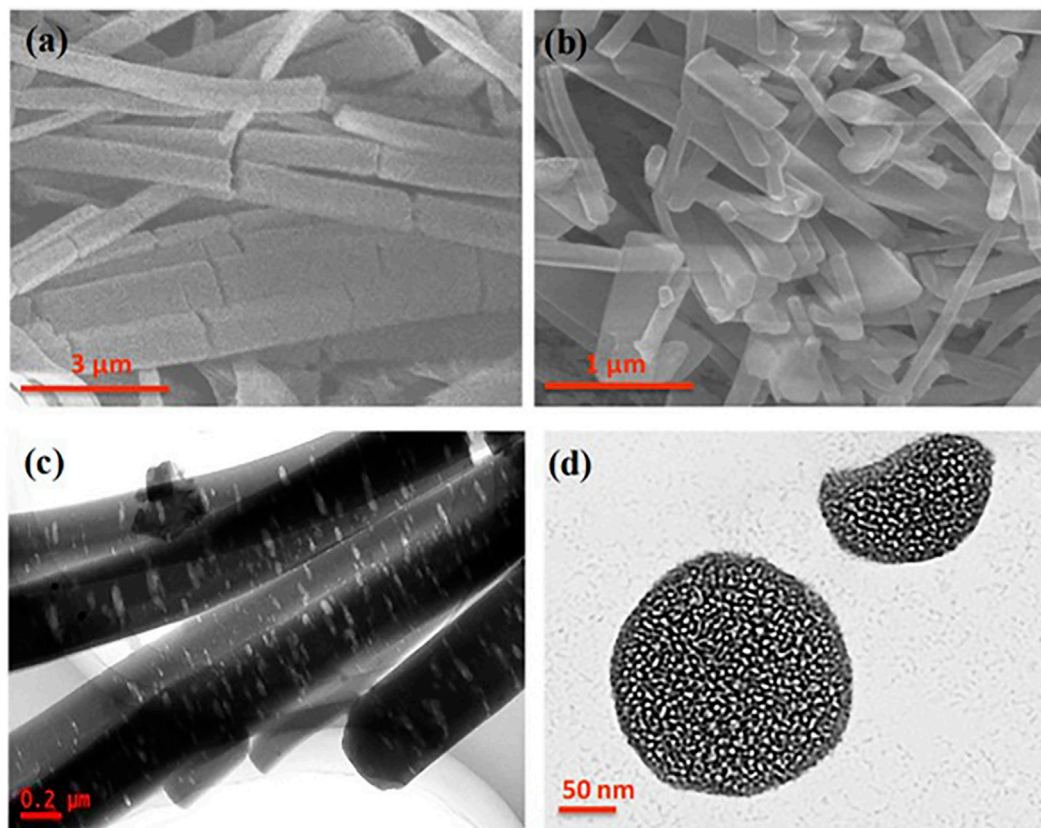


**FIGURE 2 |** (A) and (B) SEM image of RN-g-C<sub>3</sub>N<sub>5</sub>. (C) TEM image of RN-g-C<sub>3</sub>N<sub>5</sub>. (D) TEM image of a cross section of RN-g-C<sub>3</sub>N<sub>5</sub>. Reproduced with permission from (Wang et al., 2019).

hydrazine hydrate solution at 140°C for 24 h. Then, the obtained solid was annealed at 450°C for 2 h. The obtained material presented C<sub>3</sub>N<sub>5</sub>, determined by XPS, and with a band gap of 1.76 eV. The chemical structure was elucidated by ss-<sup>13</sup>C NMR using the cross-polarization magic-angle spinning (CPMAS) and XRD. The C<sub>3</sub>N<sub>5</sub> CPMAS-NMR spectrum showed two peaks at 164 and 156 ppm for N<sub>2</sub>C=N=N- and CN<sub>3</sub> carbons, respectively. CRD pattern of C<sub>3</sub>N<sub>5</sub> showed the typical broad 002 peak at 27.6° corresponding to the 0.33 nm interplanar layer distance. Photoelectrochemical water splitting experiments were carried out using Na<sub>2</sub>S as hole scavenger and C<sub>3</sub>N<sub>5</sub>-sensitized TiO<sub>2</sub> as photoelectrode. This achieved a photocurrent density of 465 μA/cm<sup>2</sup> under AM 1.5 G irradiation, while under identical conditions, the value of photocurrent density using g-C<sub>3</sub>N<sub>4</sub> sensitized TiO<sub>2</sub> was only of 373 μA/cm<sup>2</sup>. The improved photoelectrochemical activity was attributed to the position of the valence band in C<sub>3</sub>N<sub>5</sub> (+1.04 V vs. NHE) in comparison with g-C<sub>3</sub>N<sub>4</sub> (+1.8 V vs. NHE) together with the photosensitizing behavior of C<sub>3</sub>N<sub>5</sub> at longer wavelengths (505 nm) than that of g-C<sub>3</sub>N<sub>4</sub> due to the reduced band gap. The same synthetic protocol was used by Yin et al. to prepare C<sub>3</sub>N<sub>5</sub>/Ag<sub>3</sub>PO<sub>4</sub> heterojunctions, and the photocatalytic removal of tetracycline hydrochloride (TCH) was investigated (Yin et al., 2021).

Recently, P-doped C<sub>3</sub>N<sub>5</sub> nanosheets have been synthesized using 3-amino-1H-1,2,4-triazole and phosphonitrilic chloride (Liu et al., 2021). These precursors were mixed and ground before thermal condensation at 500°C for 4 h. After natural cooling, the obtained solid was annealed again at 550°C for thermal copolymerization for 4 h. In this case, two diffraction peaks appeared in the XRD measurements, attributed to in-plane packing in the 001 plane and the interlayer stacking along the 002 direction at 13.2° and 27-7°, respectively. These peaks did not shift after P-doping, indicating that the structure of C<sub>3</sub>N<sub>5</sub> is preserved. The obtained P-doped C<sub>3</sub>N<sub>5</sub> photocatalyst was used in the photocatalytic RhB degradation. The photocatalytic efficiency for RhB degradation values obtained with the P-doped C<sub>3</sub>N<sub>5</sub> was higher than the values reported in previous studies using doped g-C<sub>3</sub>N<sub>4</sub> or its composites.

## CN MATERIALS (C<sub>1</sub>N<sub>1</sub> OR C<sub>3</sub>N<sub>3</sub>)

C<sub>1</sub>N<sub>1</sub> is a porous polymeric carbon nitride comprising pores formed by three carbon atoms and three nitrogen atoms. The pores of ca. 3.4 Å of diameter are highly polar, which makes them excellent candidates to chelate metals and adsorb small molecules. Moreover, Srinivasu et al. reported in 2014 using

first-principle calculations that a monolayer C<sub>1</sub>N<sub>1</sub> structure have a band gap of 2.89 eV, which decreases to 2.75 eV in a multilayered structure, and studied the potential of the simulated C<sub>1</sub>N<sub>1</sub> structure and different doped derivatives as photocatalysts (Srinivasu et al., 2014).

Though synthetic efforts to produce polymeric C<sub>1</sub>N<sub>1</sub> can be found as early as in the 1800s when scientists condensed metal cyanides (i.e., production of paracyan), the advances in technology did not allow then to characterize whether the produced materials were crystalline or had a good photocatalytic response (Lopez-Salas et al., 2020). Surprisingly, despite the potential of C<sub>1</sub>N<sub>1</sub> materials, the amount of reported cases of successful C<sub>1</sub>N<sub>1</sub> syntheses is still very limited. In 2004, Gao et al. reported for the first time the preparation of tubular luminescent polymeric protonated C<sub>3</sub>N<sub>3</sub> networks (i.e. [(C<sub>3</sub>N<sub>3</sub>)<sub>2</sub>(NH)<sub>3</sub>]<sub>n</sub>) through a solvothermal route involving the reaction of C<sub>3</sub>N<sub>3</sub>Cl<sub>3</sub> with NH<sub>4</sub>Cl in the presence of a little iron powder at 300°C (Guo et al., 2004). The tubular structures formed exhibited a characteristic of 002 basal plane diffraction peak in XRD diffractogram and comprised triazine rings according to FTIR. The luminescent and UV-vis absorption characteristics pointed at π-π\* electronic transitions.

Soon afterward, the same group reported for the first time the synthesis of graphite-like lamellar C<sub>1</sub>N<sub>1</sub> structures through the Wurtz reaction of C<sub>3</sub>N<sub>3</sub>Cl<sub>3</sub> in molten alkali metals (Na, K) (Guo et al., 2005; Yin et al., 2017). The obtained materials showed different compositions (i.e., g-CN<sub>1.20</sub>, g-CN<sub>0.96</sub>, and g-CN<sub>0.25</sub>) depending on the synthetic temperature used (220°C, 300°C, and 380°C, respectively). All samples exhibited at 002 diffraction peak in their XRD patterns, but sample g-CN<sub>0.96</sub> showed poor crystallinity compared with samples prepared at 220°C and 380°C, and the authors suggested post-treatments (such as annealing) to improve its crystallization. However, such treatment would only lead to composition changes. Moreover, the structures showed weak SAED diffraction rings indicating the disorder of the lamellar microstructure of the samples.

A time gap was given from these last results until the next C<sub>1</sub>N<sub>1</sub>-like structures were reported. In 2014, Liu et al. reported the preparation of similar materials by the trimerization of 2,4,6-tricyano-1,3,5-triazine in molten ZnCl<sub>2</sub> (to avoid evaporation) at 400°C (Liu et al., 2014). The produced polymers had a multilayered 2D shape and virtually no accessible surface area as shown by nitrogen adsorption-desorption isotherms at 77 K. In 2017, H. Yin et al. used the method of Guo to prepare C<sub>3</sub>N<sub>3</sub> from C<sub>3</sub>N<sub>3</sub>Cl<sub>3</sub> in the presence of NaCl in autoclaves. The materials showed the typical 002 basal plane diffraction, comprised triazine rings, and had a C:N ratio of 1. Again, the materials exhibited poor N<sub>2</sub> adsorption uptake according to N<sub>2</sub> adsorption-desorption isotherm at 77 K. Interestingly, the material Coulombic efficiency was enhanced at 600°C and the C<sub>3</sub>N<sub>3</sub> products were used in Li-ion batteries. Probably due to the large heat treatment temperature, Yin and coworkers obtained black products and did not report on the color of the obtained material or their absorption properties. Also, Liu et al. did not investigate further in this regard.

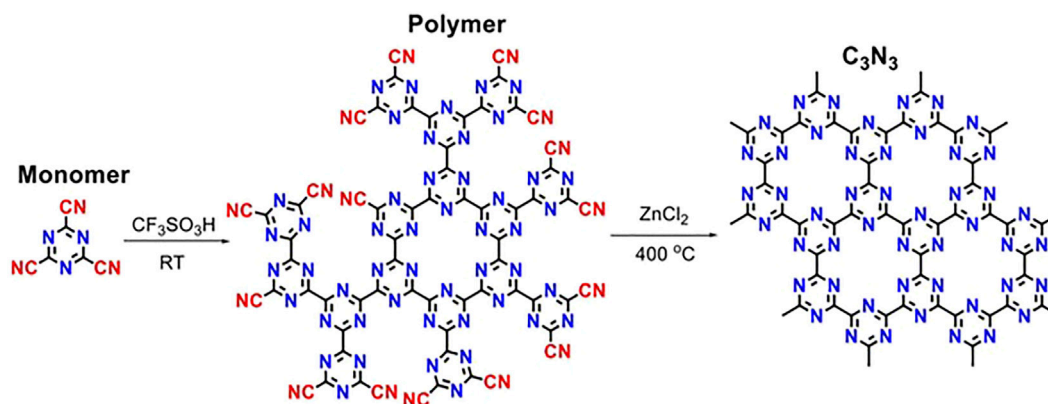
In 2019, C<sub>3</sub>N<sub>3</sub> frameworks obtained from 2,4,6-tricyano-1,3,5-triazine also using an ionothermal approach were also reported by J. Zheng et al. (Scheme 2) (Zeng et al., 2019). They used a pre-

polymerization step in triflic acid and then a heat treatment in ZnCl<sub>2</sub> at 400°C for 6 days. The resulting material showed two broad peaks at 14.10° and 27.25° corresponding to 100 and 002 reflections of A-B stacking of layered C<sub>3</sub>N<sub>3</sub> ordered structures (with unit parameters a = b = 7.25 Å and c = 6.64 Å). The materials were then coordinated with FeCl<sub>3</sub> and used as oxygen reduction electrocatalysts. Also in 2019, S. Fenetti et al. reported the preparation under high-pressure conditions of C<sub>6</sub>N<sub>6</sub>-like materials using 2,4,6-tricyano-1,3,5-triazine as a precursor (Fanetti et al., 2019). The behavior of the precursor under different temperature and pressure conditions was analyzed. Synchrotron x-ray diffraction suggested the presence of layered carbon nitride domains or structurally disordered nanocrystalline phases within the sample. More recently, a synthetic route to produce high-quality C<sub>3</sub>N<sub>3</sub> materials in a relatively larger scale was reported by J. Feng and M. Li (Feng and Li, 2020). They used the Ullman reaction to also polymerize cyanuric chloride (C<sub>3</sub>N<sub>3</sub>Cl<sub>3</sub>) on top of a copper foil. In the paper, the authors describe how using copper films is much advantageous than the previously reported synthetic methods because copper promotes the formation of radical instead of anionic intermediates, which favor the formation of large amounts of crystalline products, can migrate into the material matrix, and allow layer by layer growth of C<sub>3</sub>N<sub>3</sub> (Figure 3). The reaction was optimized at 260°C, and a gray layer on top of the copper film was produced, which already pointed at the formation of a photoactive material. Before acid washing, the sample is crystalline, and its XRD pattern corresponds to (C<sub>3</sub>N<sub>3</sub>)·(CuCl). However, acid washing leads to the loss of crystallinity of the sample.

Copper-anchored C<sub>3</sub>N<sub>3</sub> frameworks exhibited a much lower electrochemical overpotential for the hydrogen evolution reaction (306 mV vs. RHE at 10 mA cm<sup>-2</sup>) than the acid washed sample (533 mV vs. RHE at 10 mA cm<sup>-2</sup>). Due to its calculated bandgap of 2.2 eV, the authors also ran experiments using light excitation with a 300-W Xe lamp with a 420-nm filter in 1 M KOH electrolyte, with Ag/AgCl as reference electrode and a graphite rod as counter electrode. Photoelectrochemical reduction of hydrogen over copper-anchored C<sub>3</sub>N<sub>3</sub> occurred with even lower overpotential (256 mV vs. RHE at 10 mA cm<sup>-2</sup>) probing the photoactivity of the material. Moreover, chopping light experiments showed that current increased sharply when light was on indicating that charge recombination was negligible. All in all, the results of copper-loaded C<sub>3</sub>N<sub>3</sub> indicated that these materials are very promising photocatalysts. However, more research efforts are necessary to further produce pure C<sub>3</sub>N<sub>3</sub> networks and explore the difference in the photoelectrochemical response that different dopants induce in the frameworks.

## C<sub>2</sub>N

C<sub>2</sub>N is probably the member of the carbon nitride family that has attracted more attention in the last years. C<sub>2</sub>N is also a porous material, and as for C<sub>1</sub>N<sub>1</sub>, its structure has electron-rich 6 N-pores that are predicted to anchor metals and adsorb small molecules (Du et al., 2016; He et al., 2016; Bhattacharyya et al., 2018; Qin et al., 2018). In 2015, Mahmood et al.



**Scheme 2** | Reaction mechanism to produce C<sub>3</sub>N<sub>3</sub> from 2,4,6-tricyano-1,3,5-triazine. Reproduced with permission from Zeng et al. (2019).

reported for the first time the preparation of layered two-dimensional C<sub>2</sub>N *via* a simple wet-chemical reaction (Mahmood et al., 2015). The material was prepared by simply mixing hexaaminobenzene (HAB) trihydrochloride and hexaketocyclohexane (HKH) octahydrate in N-methyl-2-pyrrolidone and using a few drops of acid as catalyst. Moreover, the resulting material was dark black in color and exhibited calculated and experimental bandgaps of ca. 1.70 and 1.96 eV, respectively (Figure 4) which points at this material as an excellent photocatalyst. The material was used to prepare a field-effect transistor device fabricated that exhibited an on/off ratio of 10<sup>7</sup>.

Ever since it was synthesized for the first time, reports on using C<sub>2</sub>N materials have flourished (Tian et al., 2020), and the synthetic routes to produce C<sub>2</sub>N have been also described elsewhere (Tian et al., 2020; Tan et al., 2021). However, experimental reports describing the photocatalytic activity of C<sub>2</sub>N are still rare. In 2018, Lei Wang et al. reported the preparation of Z-scheme overall water splitting C<sub>2</sub>N and aza-fused microporous polymeric (aza-CMP) ultrathin nanosheet photocatalysts (Wang L. et al., 2018). Simultaneous evolution of H<sub>2</sub> and O<sub>2</sub> with a molar ratio of 2:1 was observed with a maximum H<sub>2</sub> production rate of 5 μmol/h under irradiation of a 300-W Xe lamp filtered at 420 nm, and a solar-to-hydrogen conversion efficiency of 0.23% with quantum efficiency of 4.3% at 600 nm. C<sub>2</sub>N was prepared as described by Mahmood, and none of the two polymers was able to catalyze the overall water splitting under visible light when used independently. However, the aza-CMP/C<sub>2</sub>N heterojunctions were obtained by mixing and annealing the two types of nanosheets. Comparison of the N K-edge XANES spectra of aza-CMP, C<sub>2</sub>N, and aza-CMP/C<sub>2</sub>N indicated the formation of the junctions. Different aza-CMP/C<sub>2</sub>N ratios were used and the final heterojunctions were able to produce H<sub>2</sub> and O<sub>2</sub> in a 2:1 stoichiometric ratio (Figure 5).

Interestingly, based on the already reported results on aza-CMP-C<sub>2</sub>N Z-schemes, Y. Fan et al. reported that the same heterojunctions hold a great potential as photocatalysts for the CO<sub>2</sub> reduction reaction as calculated by first-principle computations (Fan et al., 2021). However, still there are no more experimental evidences of the performance of C<sub>2</sub>N or C<sub>2</sub>N heterojunctions as photocatalysts.

In 2019, X. Zhang et al. reported 41%–56% exfoliation yields for C<sub>3</sub>N<sub>4</sub>, C<sub>2</sub>N, and aza-CMP in acid media (Zhang et al., 2019). In their work, C<sub>2</sub>N was also synthesized using HAB and HKH in NMP. However, sonication of the materials in 1 M HCl or 12 M HCl solutions yielded 5-nm-thick C<sub>2</sub>N layers that remain suspended stably for months. No peak shift was observed by PXRD before and after exfoliation, and thus, the authors hypothesized that the exfoliation took place through a delamination process facilitated by water molecules and not induced *via* Brønsted acid intercalation. Moreover, all the samples exhibited similar N K-edge XANES and N1s XPS spectra and unchanged <sup>1</sup>H MAS solid-state NMR, indicating that the structures remain intact after the treatment. The photo-response of the exfoliated C<sub>2</sub>N was fivefold larger than g-C<sub>3</sub>N<sub>4</sub> in water/triethanolamine solution under visible light (λ ≥ 420 nm) with a 300-W Xe lamp (100 mW/cm<sup>2</sup>), as chopping light experiments indicated. Moreover, the sample response was very stable after cycling (Figure 6).

## C<sub>3</sub>N

The crystalline structure of C<sub>3</sub>N, as well as its electronic configuration, was first predicted in 2012 (Hu et al., 2012), and this attracted immediately the attention of the scientific community as a consequence of its semiconductor behavior, their optoelectronic properties, high specific surface area, among other chemical, and physical characteristics. Since then, a considerable number of theoretical studies have investigated its mechanical, electronic, optical, structural, etc., characteristics in different configurations, such as monolayer, bilayer, bulk, or alternatively, modifying the crystalline structure with defects in the form of vacant, voids, or heteroatom doped (Wang X. et al., 2018; Shi et al., 2018; Shirazi et al., 2018; Tagani, 2018; Wu et al., 2018). However, only a few papers have reported synthetic procedures to obtain crystalline C<sub>3</sub>N, and as consequence, the direct application of this material in photocatalysis has not been explored so far to the best of our knowledge, despite theoretical calculations having predicted its suitability.

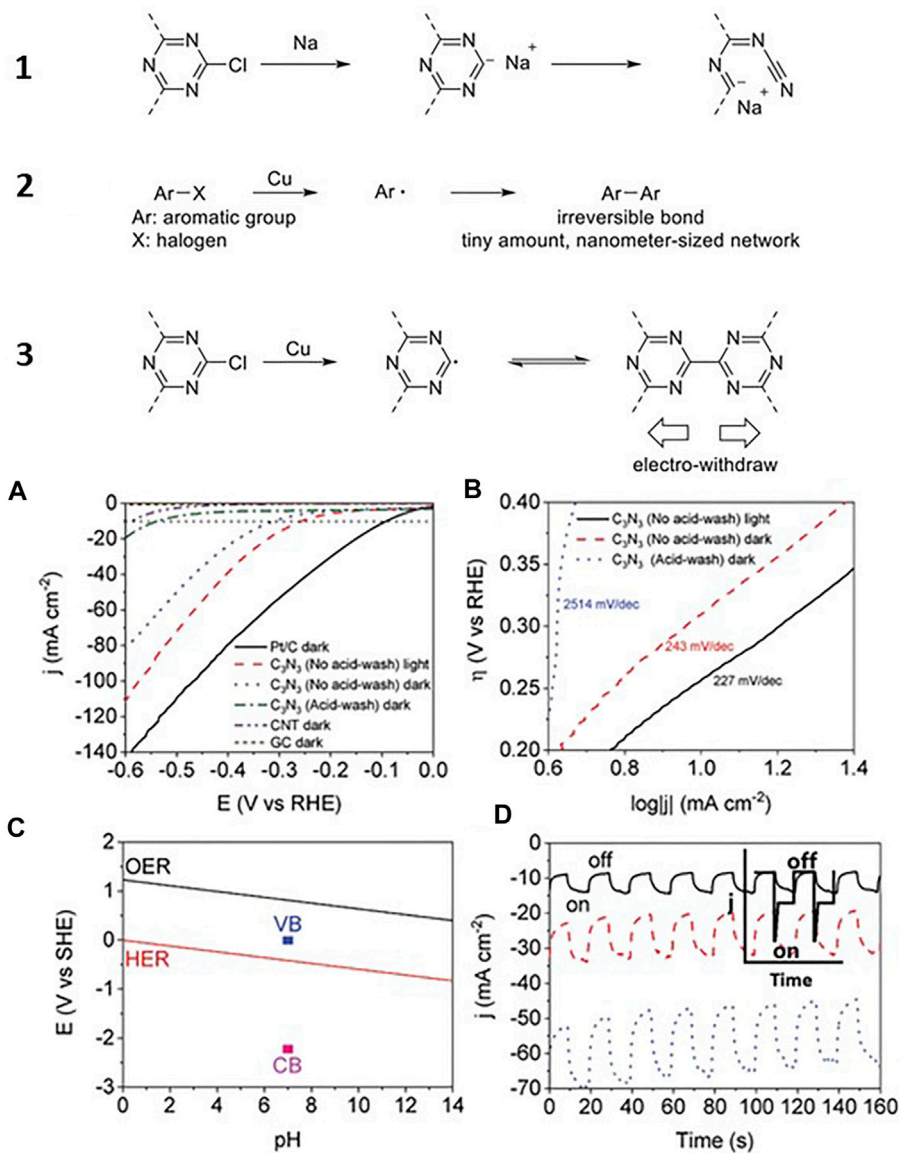


**FIGURE 3 | (Top panel)** Different reaction mechanisms followed to prepare C<sub>1</sub>N<sub>1</sub> materials. **(bottom panel)** (A) Comparing linear sweep voltammetry curves of different electrodes in dark or under light; (B) Tafel curves of C<sub>3</sub>N<sub>3</sub> electrodes between 0.2 and 0.4 V vs. RHE; (C) comparing red-ox coupling for water splitting, valence band (VB), and conduction band (CB) of C<sub>3</sub>N<sub>3</sub> before acid wash (OER: oxygen evolution reaction); (D) Chronoamperometric data of C<sub>3</sub>N<sub>3</sub> under chopped light [from top to bottom: -0.28, -0.38, and -0.48 V vs. RHE; the inset shows the recombination of photoelectrons and holes for reported catalysts (25)]. Reproduced with permission from Feng and Li (2020).

Encouraged by the striking properties predicted by theoretical calculations, bulk C<sub>3</sub>N was first prepared from the thermolysis of *m*-phenylenediamine at 800°C under static vacuum for 7–9 days by King et al. in 2013 (King et al., 2013). In this preparation method, hollow carbon microspheres in the absence of N atoms were also obtained. XRD measurements showed two broad signals at 26° and 44° corresponding to the 002 and 100 facets, respectively, indicating that the C<sub>3</sub>N possess multi-layered turbostratic graphitic arrangement without periodic ordering between each C<sub>3</sub>N layer. XPS analysis confirmed that the flakes contained a substantial amount of nitrogen, obtaining an empirical formula of C<sub>3.33</sub>N. The

excess of C atoms from the ideal composition was attributed to contamination from the microspheres.

Lately, Baek and co-workers reported in 2016 the synthesis of 2D C<sub>3</sub>N crystals from the direct pyrolysis of hexaaminobenzene trihydrochloride (HAB) single crystals at 500°C for 2 h (Mahmood et al., 2016b). They studied in detail the C<sub>3</sub>N formation mechanism, which involved the evolution of ammonia and ammonium chloride, following Eq. 1. The C<sub>3</sub>N chemical composition was confirmed by XPS, which was in good agreement with the theoretical calculations performed so far. They also characterized the structure by solid state <sup>13</sup>C NMR (ss-

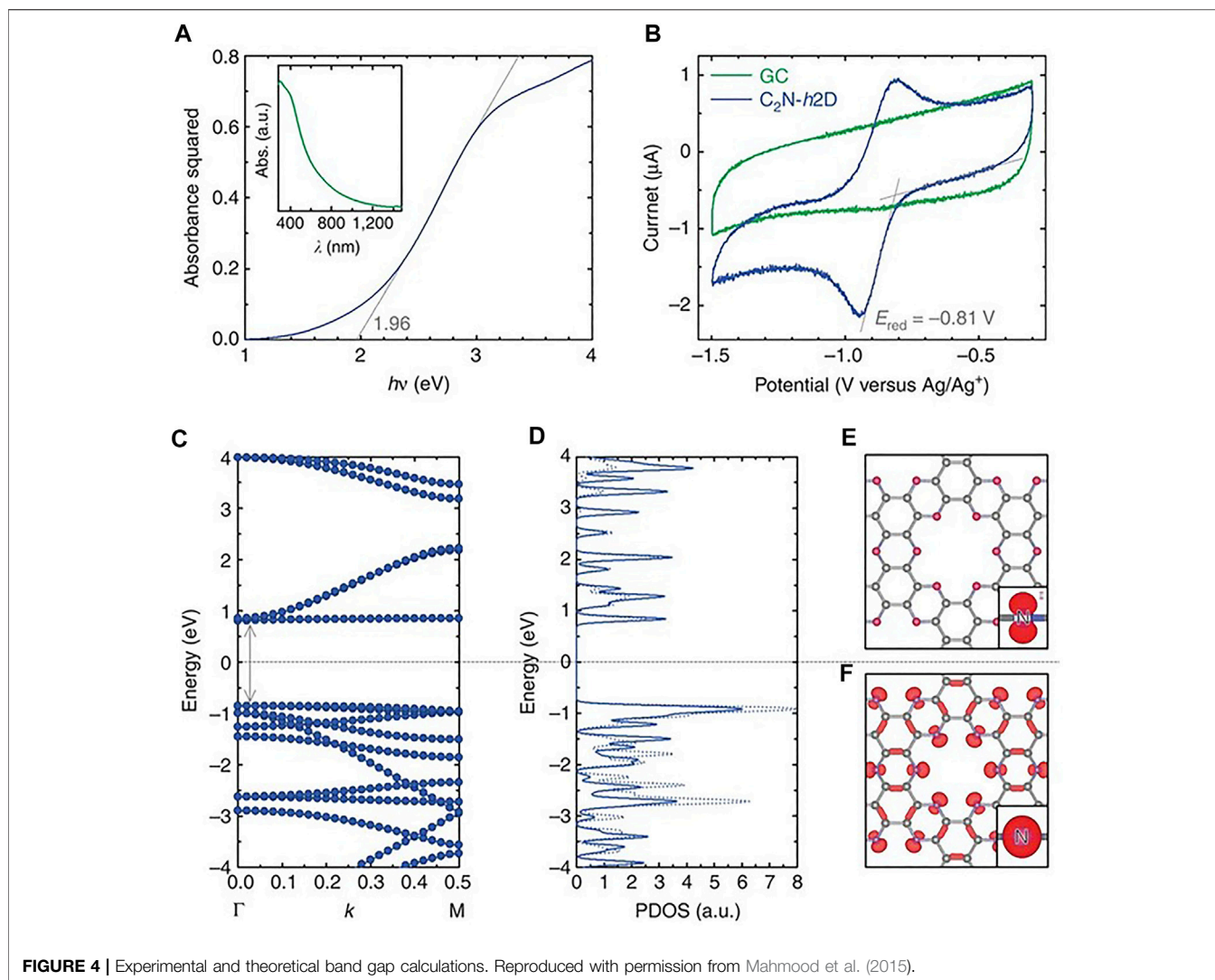


**FIGURE 4** | Experimental and theoretical band gap calculations. Reproduced with permission from Mahmood et al. (2015).

<sup>13</sup>C NMR), obtaining only two characteristic peaks of 150.80 and 126.02 ppm, attributed to carbon atoms bonded to tertiary nitrogen and carbon atoms linked to primary or secondary amines, respectively. In this case, XRD revealed three major peaks at 12.8°, 26.1°, and 44.7° corresponding to *d* spacing of 6.87 Å, 3.40 Å, and 2.02 Å, respectively. The peak at 26.1° was attributed to the interlayer *d* spacing (3.40 Å) of the obtained material. This crystallographic result was in good agreement with the simulated XRD patterns after Pawley refinement. The electrical properties of the as-prepared C<sub>3</sub>N were also investigated, and a conductivity of 0.72 S/cm was determined, which makes this material an ideal candidate for opto-electronic applications.



In the same year, Lazauskas and coworkers reported the synthesis of C<sub>3</sub>N thin films from polymeric C<sub>x</sub>N<sub>y</sub> powder thermal evaporation (Lazauskas et al., 2016). The C<sub>x</sub>N<sub>y</sub> precursor was obtained through a two-step synthetic

procedure by direct urea thermal treatment at 300°C for 3 h, and after fine grinding and milling, the obtained material was heated again at 520°C for 4 h. XRD analysis determined that during the first thermal treatment, urea decomposed to biuret, which subsequently also decomposed, evolving to cyanuric acid. In the second thermal treatment at 520°C, cyanuric acid decomposes to ammelide, ammeline, and melamine at temperatures below 400°C. At larger temperatures, these compounds evolved to polymeric C<sub>x</sub>N<sub>y</sub>. The obtained material was characterized by an orthorhombic crystal structure and an A–B layers staking. Finally, C<sub>3</sub>N thin films were deposited on arbitrary substrates by thermal vacuum deposition of the polymeric C<sub>x</sub>N<sub>y</sub> at 10<sup>−6</sup> mbar and 1 Å/s rate. The chemical composition and structure were determined by XRD, XPS, FTIR, and Raman spectroscopy. XRD pattern showed a broad peak at 23.7°, indicating the presence of dispersed polymeric C<sub>x</sub>N<sub>y</sub> fragments. The authors suggested that during thermal vacuum deposition, the polymeric C<sub>x</sub>N<sub>y</sub> is fragmented, and the previously observed crystallinity is no longer observed in the thin films. The composition was determined by XPS, obtaining a surface atomic

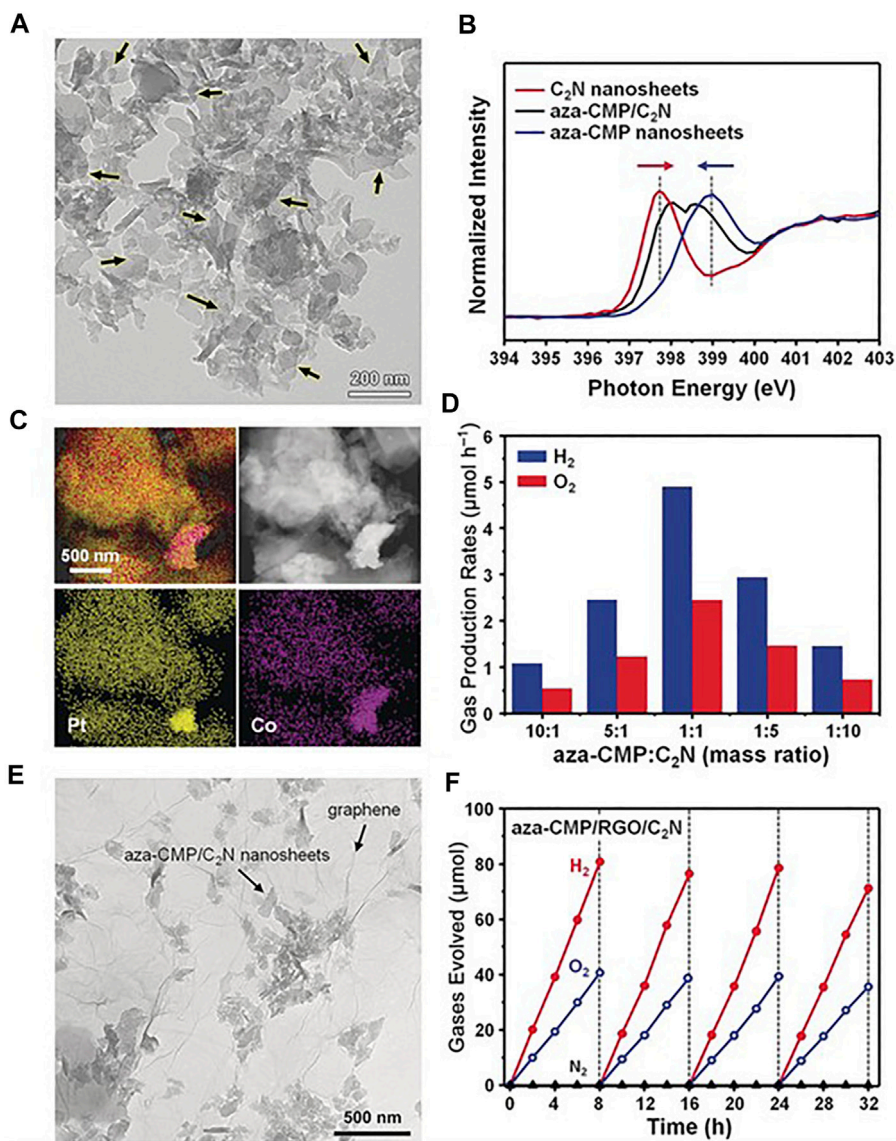
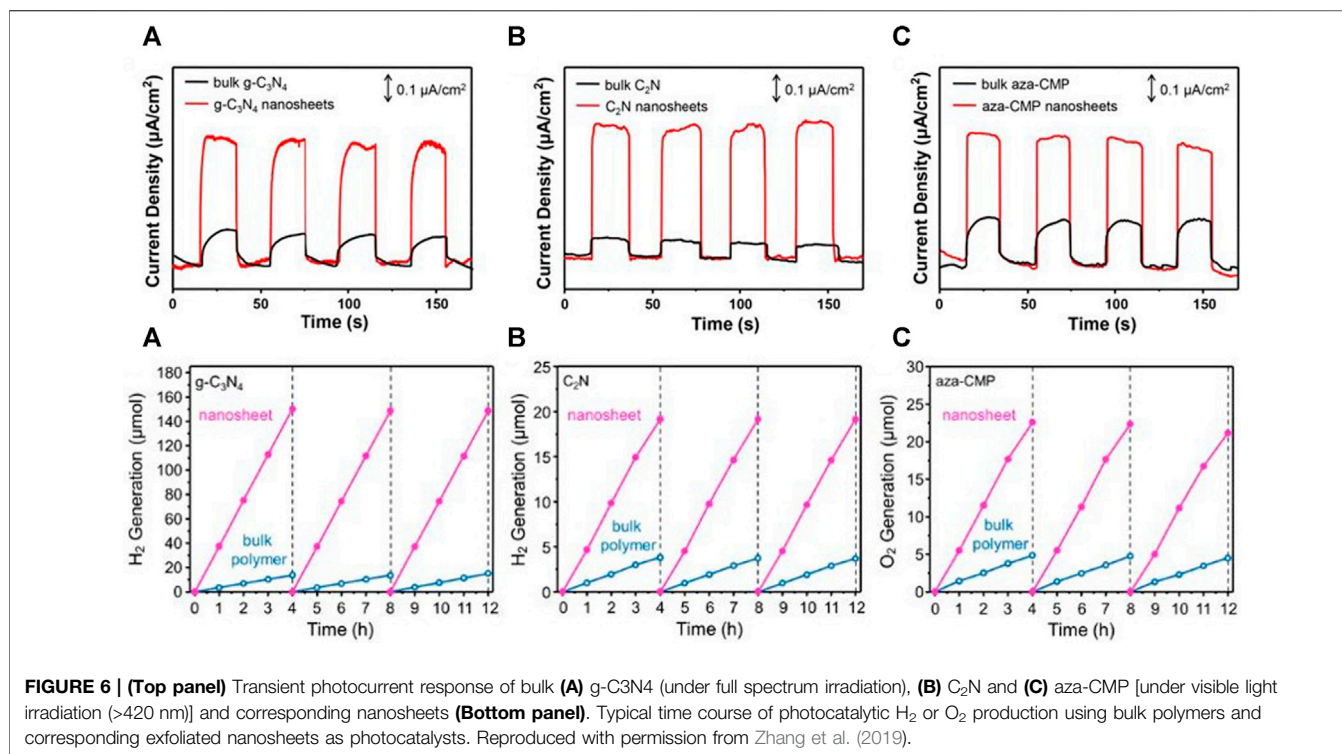


**FIGURE 5 | (A)** TEM image of aza-CMP/C<sub>2</sub>N heterostructures. Arrows indicate overlapped interfaces. **(B)** The N K-edge XANES spectra of aza-CMP, C<sub>2</sub>N, and aza-CMP/C<sub>2</sub>N. **(C)** HAADF-STEM images and elemental mapping of heterostructures formed by Pt-labeled C<sub>2</sub>N and Co-labeled aza-CMP. **(D)** The overall water-splitting performance of aza-CMP/C<sub>2</sub>N heterostructures with different compositions. **(E)** Transmission electron microscope (TEM) image of the aza-CMP/RGO/C<sub>2</sub>N photocatalyst. **(F)** Typical time course of H<sub>2</sub> and O<sub>2</sub> production using the aza-CMP/RGO/C<sub>2</sub>N photocatalyst under visible light irradiation. Reproduced with permission from Wang L. et al. (2018).

concentration of C<sub>2.94</sub>N. UV-Vis measurements showed an absorption edge at approximately 423.2 nm, corresponding to an optical band gap of 2.93 eV.

One year later, Yang et al. reported the controllable large-scale synthesis of C<sub>3</sub>N QDs through 2,3-diaminophenazine polymerization by hydrothermal treatment (Yang et al., 2017). The polymerization steps were characterized by matrix-assisted laser desorption ionization time-of-flight mass spectroscopy (MALDI-TOFMS). Vertical and horizontal polymerization was advanced by the addition of precursor monomers leading to the formation of large C<sub>3</sub>N flakes. The

vertical polymerization consisted first in H abstraction from C–H and N–H bonds, providing C and N atoms with dangling bonds, subsequent formation of C–N bonds between the growing polymer fragment and the added monomer, and finally the release of the excess of hydrogen. The reaction for horizontal polymerization of two monomers and the whole polymerization process is depicted in **Scheme 3**. HRTEM and SAED (**Figure 7**) exhibited a well-crystallized graphene-like honeycomb structure and the two-fold hexagonal single crystal structure of C<sub>3</sub>N indicating D<sub>6h</sub>-symmetry of the N and C atoms in agreement with theoretical calculations.



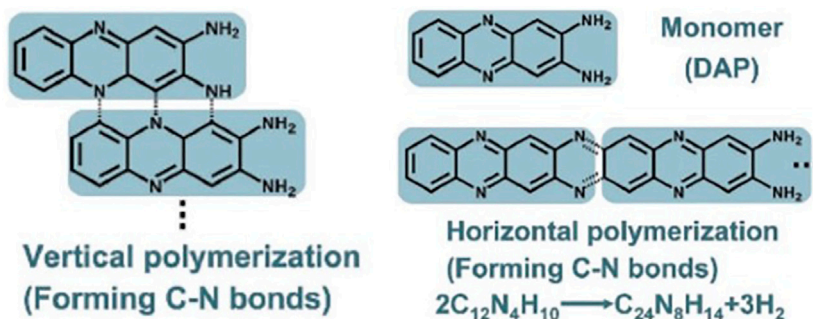
More recently, Ma et al. reported the synthesis of C<sub>3</sub>N from the imidazolate-based MOF ZIF-8 and urea (Ma et al., 2019). These two precursors (ZIF-8 and urea) were dispersed in water for 2 h, filtered and annealed at temperatures between 650 and 950°C under N<sub>2</sub> atmosphere for 2 h. The obtained carbonaceous material was, subsequently, HCl washed, filtered, and dried prior to characterization. The successful C<sub>3</sub>N composition formation was confirmed by XPS for the sample annealed at 850°C. XRD measurement showed two characteristic peaks at 25° and 43° attributed to the 002 and 100/101 diffractions of carbon, indicating the existence of disorderly oriented graphitic type fragments in the carbon matrices.

In spite of the synthetic efforts carried out to prepare crystalline C<sub>3</sub>N materials with different morphologies, only a few examples of their application in photocatalysis have been reported and are mainly based on theoretical calculations. In 2016, Baek et al. reported the band gap of C<sub>3</sub>N to be 2.6 eV (as calculated electrochemically and using scanning tunneling spectroscopy) (Mahmood et al., 2016a). Thus, it was predicted that heterostructures composed of the semiconductor materials BC<sub>3</sub> and C<sub>3</sub>N can form p-n heterojunctions with strong interlayer electron coupling and enhanced photocurrent (Zhang et al., 2018). With this in mind, Wang et al. studied the formation of BC<sub>3</sub>/C<sub>3</sub>N and BC<sub>3</sub>/BC<sub>6</sub>N van der Waals heterostructures as Z-scheme heterojunctions for photocatalytic overall water splitting by DFT calculations (Wang Z. et al., 2020). The theoretical investigations revealed that the delocalized nature of π-conjugated electrons in the monolayer components allows for high carrier mobility

between the different layers, promoting efficient photocatalytic overall water splitting. Thus, these heterojunctions were proposed as good candidates for photocatalytic water splitting. However, experimental studies confirming the simulations carried out with these heterojunctions as well as with other photocatalytic systems containing C<sub>3</sub>N have not been reported yet. Hence, the use of C<sub>3</sub>N in this area remains unexplored despite the predicted favorable optoelectronic properties.

## HETEROATOM-DOPED C<sub>x</sub>N<sub>y</sub>

Boron carbonitride (BCN) materials are inorganic semiconductors, which exhibit a lower binding energy of excitons and faster charge migration properties than other polymeric photocatalysts, such as covalent organic frameworks (COFs), conjugated microporous polymers (CMPs), and graphitic carbon nitrides (g-CN). BCN are visible light-responsive semiconductors, and the band gap energy and energy levels can be easily tuned depending on the amount of carbon incorporated into the boron nitride. Recently, Yuan et al. reported the preparation of CBN and its application in photocatalytic organic transformations (Yuan et al., 2021). CBN was prepared by mixing and grinding urea, boric acid, and glucose in different proportions. Then KCl was added and ground again. The mixed precursors were heated at 1,250°C for 5 h under ammonia flow. The obtained BCN was used as visible light-responsive photocatalyst (LED light source at 420 nm, 15 W) for the coupling of halides with different synthons. It was demonstrated



**Scheme 3** | Scheme for vertical (**left**) and horizontal (**right**) polymerization of 2,3-diaminophenazine forming C–N bonds and the respective formula. Reproduced with permission from Yang et al. (2017).

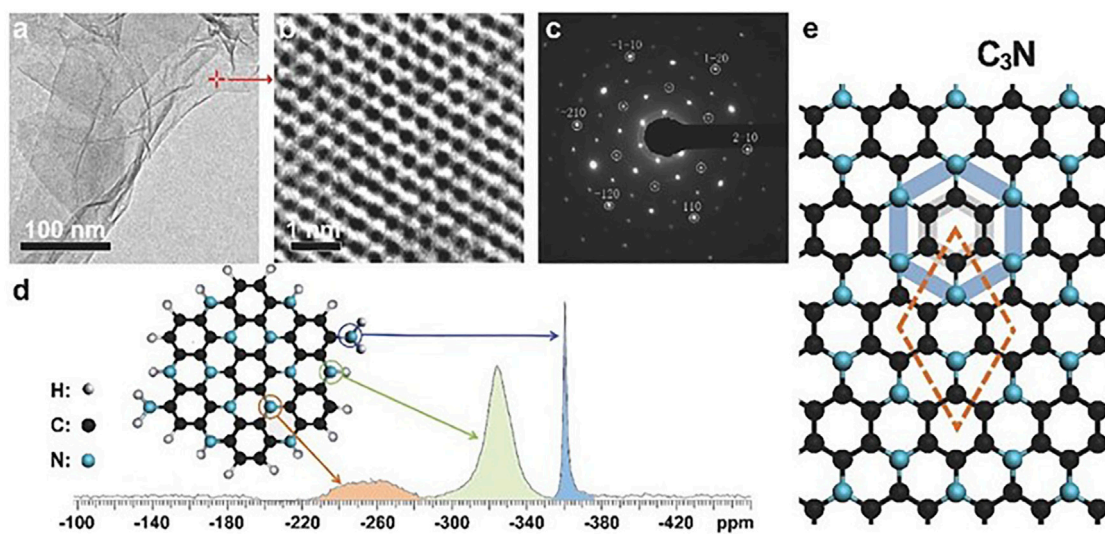


**FIGURE 7** | Structure of C<sub>3</sub>N sheets. **(A)** TEM image of a mixture of single- and multilayer C<sub>3</sub>N sheets. **(B)** Spherical aberration-corrected HRTEM image showing the honeycomb structure of a single-layer sheet marked in **(A)**. **(C)** SAED indicating the D<sub>6h</sub>-symmetry of N and C atoms in the single-layer C<sub>3</sub>N sheet. The circles mark the graphene spots and the additional spots are due to the supercell of the C<sub>3</sub>N crystal. **(D)** <sup>15</sup>N-NMR spectrum of a mixture of single-layer and multilayer C<sub>3</sub>N sheets. The assignment of the peaks to specific N atoms in the C<sub>3</sub>N crystal is indicated. **(E)** The molecular structure and supercell of the C<sub>3</sub>N crystal. The blue and black regular hexagons show the D<sub>6h</sub>-symmetry of N and C atoms in the C<sub>3</sub>N crystal, respectively. Reproduced with permission from Yang et al. (2017).

that a wide range of organic halides, including aryl-, alkyl-, bromides, and chlorides, could be reduced to carbon-centered radicals at remarkable yields.

Alternatively, Rao and coworkers reported the synthesis of BCN with two different compositions, (BN)<sub>0.75</sub>C<sub>0.25</sub> and (BN)<sub>0.3</sub>C<sub>0.7</sub>, by varying the ratio of urea, boric acid, and activated charcoal, and heating the resultant mixture at 900°C in N<sub>2</sub> atmosphere (Singh et al., 2018). The photocatalytic activity of these materials forming composites with MoS<sub>2</sub> (1:2) was investigated for H<sub>2</sub> evolution. Aqueous suspensions of the two different composites containing triethanolamine (20 vol.%) were irradiated with UV-vis light with a halogen lamp (100 W). (BN)<sub>0.75</sub>C<sub>0.25</sub>/MoS<sub>2</sub> composite showed the highest H<sub>2</sub> production rate (6,965 μmol/g·h).

Barrio et al. reported the preparation of C<sub>3</sub>N<sub>3</sub>O and its photocatalytic activity toward RhB degradation (Barrio et al., 2019). C<sub>3</sub>N<sub>3</sub>O photocatalyst was synthesized by means of the preparation of tri-aminopyrimidine-cyanuric acid supramolecular assemblies by mixing both monomers in a 1:1 molar ratio and subsequent calcination at low temperatures (300–400°C). C<sub>3</sub>N<sub>3</sub>O calcined at 400°C exhibited a 2.17 eV band gap with a conduction band maximum (CBM) suitable for CO<sub>2</sub> reduction, while the C<sub>3</sub>N<sub>3</sub>O calcined at 300°C presented a 1.41 eV band gap with CBM above the H<sup>+</sup> reduction potential, but not enough for CO<sub>2</sub> reduction. Thus, the photocatalytic activity for these two materials for RhB degradation was tested under visible light illumination (λ ≥ 410 nm), and C<sub>3</sub>N<sub>3</sub>O calcined at 400°C showed the highest photoactivity, while C<sub>3</sub>N<sub>3</sub>O calcined at 300°C presented negligible activity.

## FUTURE CHALLENGES AND OPPORTUNITIES

The different experimental procedures developed for the synthesis of C<sub>x</sub>N<sub>y</sub> materials are in its infancy. For instance, the majority of the synthetic routes are based in either expensive or toxic compounds, and the material processability is still very limited. Thus, one of the main current challenges for researchers working on the field is to find new and scalable strategies to produce these materials.

Regarding their application as photocatalysts, some of the performance of the materials have been theoretically predicted and simulated but, not fully explored neither experimentally nor theoretically yet. For instance, majority of the reports on the photocatalytic performance of C<sub>x</sub>N<sub>y</sub>s focus on water splitting. However, theoretical calculations predict that heteroatom-doped C<sub>x</sub>N<sub>y</sub>, as well as heterojunctions with other 2D materials, promote important differences in the final material band gap, which forecast a great potential of the C<sub>x</sub>N<sub>y</sub> family in a broader spectrum of photocatalytic reactions. Moreover, the porous nature of some of the materials (i.e., C<sub>1</sub>N<sub>1</sub> or C<sub>2</sub>N) can facilitate the adsorption of certain molecules extending the limits of the photocatalytic activity of the materials from only

water splitting to more complex water purification systems. In this regard, we also expect material processability (for example, in the form of nanoribbons, thin films, powders, and quantum dots) to have a great impact in the overall performance as photocatalysts (i.e., facilitating the creation of defects or heteroatom doping itself).

Overall, we envision that C<sub>x</sub>N<sub>y</sub> materials will be extensively used as photocatalysts for a variety of reactions in the near future. However, strong efforts are still needed so the possibilities of these materials are fully explored, their limits understood, and they are produced through scalable synthetic routes.

## AUTHOR CONTRIBUTIONS

All authors listed have made a substantial, direct, and intellectual contribution to the work and approved it for publication.

## FUNDING

The Max Planck Society is greatly acknowledged for the funding support.

## REFERENCES

- Albero, J., Mateo, D., and García, H. (2019). Graphene-Based Materials as Efficient Photocatalysts for Water Splitting. *Molecules* 24, 906. doi:10.3390/molecules24050906
- Bafekry, A., Shayesteh, S. F., and Peeters, F. M. (2019). Two-dimensional Carbon Nitride (2DCN) Nanosheets: Tuning of Novel Electronic and Magnetic Properties by Hydrogenation, Atom Substitution and Defect Engineering. *J. Appl. Phys.* 126, 215104. doi:10.1063/1.5120525
- Barrio, J., Karjule, N., Qin, J., and Shalom, M. (2019). Condensation of Supramolecular Assemblies at Low Temperatures as a Tool for the Preparation of Photoactive C<sub>3</sub>N<sub>3</sub>O Materials. *ChemCatChem* 11, 6295–6300. doi:10.1002/cctc.201901485
- Bhattacharyya, K., Pratik, S. M., and Datta, A. (2018). Controlled Pore Sizes in Monolayer C<sub>2</sub>N Act as Ultrasensitive Probes for Detection of Gaseous Pollutants (HF, HCN, and H<sub>2</sub>S). *J. Phys. Chem. C* 122, 2248–2258. doi:10.1021/acs.jpcc.7b11963
- Chu, C., Zhu, Q., Pan, Z., Gupta, S., Huang, D., Du, Y., et al. (2020). Spatially Separating Redox Centers on 2D Carbon Nitride with Cobalt Single Atom for Photocatalytic H<sub>2</sub>O<sub>2</sub> Production. *Proc. Natl. Acad. Sci. USA* 117 (12), 6376–6382. doi:10.1073/pnas.1913403117
- Du, J., Xia, C., Xiong, W., Zhao, X., Wang, T., and Jia, Y. (2016). Tuning the Electronic Structures and Magnetism of Two-Dimensional Porous C<sub>2</sub>N via Transition Metal Embedding. *Phys. Chem. Chem. Phys.* 18, 22678–22686. doi:10.1039/c6cp03210a
- Fan, Y., Qi, S., Li, W., and Zhao, M. (2021). Direct Z-Scheme Photocatalytic CO<sub>2</sub> Conversion to Solar Fuels in a Two-Dimensional C<sub>2</sub>N/aza-CMP Heterostructure. *Appl. Surf. Sci.* 541, 148630. doi:10.1016/j.apsusc.2020.148630
- Fanetti, S., Nobrega, M. M., Dziubek, K., Citroni, M., Sella, A., Mcmillan, P. F., et al. (2019). Structure and Reactivity of 2,4,6-Tricyano-1,3,5-Triazine under High-Pressure Conditions. *CrystEngComm* 21, 4493–4500. doi:10.1039/c8ce02154f
- Fang, Y., and Wang, X. (2018). Photocatalytic CO<sub>2</sub> Conversion by Polymeric Carbon Nitrides. *Chem. Commun. (Camb)* 54, 5674–5687. doi:10.1039/c8cc02046a
- Feng, J., and Li, M. (2020). Large-Scale Synthesis of a New Polymeric Carbon Nitride-C<sub>3</sub>N<sub>3</sub> with Good Photoelectrochemical Performance. *Adv. Funct. Mater.* 30 (23), 2001502. doi:10.1002/adfm.202001502
- Fujishima, A., and Honda, K. (1972). Electrochemical Photolysis of Water at a Semiconductor Electrode. *Nature* 238, 37–38. doi:10.1038/238037a0
- Guo, Q., Yang, Q., Yi, C., Zhu, L., and Xie, Y. (2005). Synthesis of Carbon Nitrides with Graphite-like or Onion-like Lamellar Structures via a Solvent-free Route at Low Temperatures. *Carbon* 43, 1386–1391. doi:10.1016/j.carbon.2005.01.005
- Guo, Q., Yang, Q., Zhu, L., Yi, C., Zhang, S., and Xie, Y. (2004). A Facile One-Pot Solvothermal Route to Tubular Forms of Luminescent Polymeric Networks [(C<sub>3</sub>N<sub>3</sub>)<sub>2</sub>(NH)<sub>3</sub>]<sub>n</sub>. *Solid State. Commun.* 132, 369–374. doi:10.1016/j.ssc.2004.08.014
- Guo, Y., Li, H., Ma, W., Shi, W., Zhu, Y., and Choi, W. (2020). Photocatalytic Activity Enhanced via Surface Hybridization. *Carbon Energy* 2, 308–349. doi:10.1002/cey2.66
- Haiyan, J., Yang, L., Daohan, W., Xiaodong, H., and Bing, L. (2020). Recent Advances in Heteroatom Doped Graphitic Carbon Nitride (G-C<sub>3</sub>N<sub>4</sub>) and G-C<sub>3</sub>N<sub>4</sub>/Metal Oxide Composite Photocatalysts. *Curr. Org. Chem.* 24, 673–693.
- He, B. L., Shen, J. S., and Tian, Z. X. (2016). Iron-embedded C<sub>2</sub>N Monolayer: a Promising Low-Cost and High-Activity Single-Atom Catalyst for CO Oxidation. *Phys. Chem. Chem. Phys.* 18, 24261–24269. doi:10.1039/c6cp03398a
- Hu, Q., Wu, Q., Wang, H., He, J., and Zhang, G. (2012). First-principles Studies of Structural and Electronic Properties of Layered C<sub>3</sub>N Phases. *Phys. Status Solidi B* 249, 784–788. doi:10.1002/pssb.201147319
- Iwashina, K., Iwase, A., Ng, Y. H., Amal, R., and Kudo, A. (2015). Z-schematic Water Splitting into H<sub>2</sub> and O<sub>2</sub> Using Metal Sulfide as a Hydrogen-Evolving Photocatalyst and Reduced Graphene Oxide as a Solid-State Electron Mediator. *J. Am. Chem. Soc.* 137, 604–607. doi:10.1021/ja511615s
- Jin, X., Yang, H., Chen, N., and Qu, L. (2018). “Carbon-Based, Metal-free Catalysts for Photocatalysis,” in *Carbon-Based Metal-Free Catalysts* (Weinheim, Germany: Wiley VCH), 457–500. doi:10.1002/9783527811458.vol2-ch5
- Jin, Z., Wei, T., Huang, J., Li, F., Yang, Y., and Xu, L. (2020). Fabrication of Direct Z-Scheme Heterojunction between Zn<sub>0.5</sub>Cd<sub>0.5</sub>S and N-Rich Graphite Carbon Nitride for Boosted H<sub>2</sub> Production. *Int. J. Hydrogen Energ.* 45, 22711–22721. doi:10.1016/j.ijhydene.2020.06.093

- Kandy, M. M. (2020). Carbon-based Photocatalysts for Enhanced Photocatalytic Reduction of CO<sub>2</sub> to Solar Fuels. *Sustain. Energ. Fuels* 4, 469–484. doi:10.1039/c9se00827f
- King, T. C., Matthews, P. D., Holgado, J. P., Jefferson, D. A., Lambert, R. M., Alavi, A., et al. (2013). A Single-Source Route to Bulk Samples of C<sub>3</sub>N and the Co-evolution of Graphitic Carbon Microspheres. *Carbon* 64, 6–10. doi:10.1016/j.carbon.2013.04.043
- Kou, C., Tian, Y., Gao, L., Lu, M., Zhang, M., Liu, H., et al. (2020). Theoretical Design of Two-Dimensional Carbon Nitrides. *Nanotechnology* 31, 495707. doi:10.1088/1361-6528/abb334
- Kumar, P., Vahidzadeh, E., Thakur, U. K., Kar, P., Alam, K. M., Goswami, A., et al. (2019). C<sub>3</sub>N<sub>5</sub>: A Low Bandgap Semiconductor Containing an Azo-Linked Carbon Nitride Framework for Photocatalytic, Photovoltaic and Adsorbent Applications. *J. Am. Chem. Soc.* 141, 5415–5436. doi:10.1021/jacs.9b00144
- Lakhi, K. S., Park, D.-H., Al-Bahily, K., Cha, W., Viswanathan, B., Choy, J.-H., et al. (2017). Mesoporous Carbon Nitrides: Synthesis, Functionalization, and Applications. *Chem. Soc. Rev.* 46, 72–101. doi:10.1039/c6cs00532b
- Lazauskas, A., Baltusaitis, J., Puodžiukynas, L., Andrulevičius, M., Bagdžiūnas, G., Volyniuk, D., et al. (2016). Characterization of Urea Derived Polymeric Carbon Nitride and Resultant Thermally Vacuum Deposited Amorphous Thin Films: Structural, Chemical and Photophysical Properties. *Carbon* 107, 415–425. doi:10.1016/j.carbon.2016.06.019
- Li, M., Lu, Q., Liu, M., Yin, P., Wu, C., Li, H., et al. (2020). Photoinduced Charge Separation via the Double-Electron Transfer Mechanism in Nitrogen Vacancies G-C<sub>3</sub>N<sub>5</sub>/BiOBr for the Photoelectrochemical Nitrogen Reduction. *ACS Appl. Mater. Inter.* 12, 38266–38274. doi:10.1021/acami.0c11894
- Liu, L., Xia, Y., and Zhang, J. (2014). Design and Synthesis of Nitrogen-Rich Carbonaceous Two-Dimensional Polymer. *RSC Adv.* 4, 59102–59105. doi:10.1039/c4ra09272d
- Liu, R., Chen, Z., Yao, Y., Li, Y., Cheema, W. A., Wang, D., et al. (2020a). Recent Advancements in G-C<sub>3</sub>N<sub>4</sub>-Based Photocatalysts for Photocatalytic CO<sub>2</sub> Reduction: a Mini Review. *RSC Adv.* 10, 29408–29418. doi:10.1039/d0ra05779g
- Liu, T., Yang, G., Wang, W., Wang, C., Wang, M., Sun, X., et al. (2020b). Preparation of C<sub>3</sub>N<sub>5</sub> Nanosheets with Enhanced Performance in Photocatalytic Methylene Blue (MB) Degradation and H<sub>2</sub>-Evolution from Water Splitting. *Environ. Res.* 188, 109741. doi:10.1016/j.envres.2020.109741
- Liu, X., Xing, S., Xu, Y., Chen, R., Lin, C., and Guo, L. (2021). 3-Amino-1,2,4-triazole-derived Graphitic Carbon Nitride for Photodynamic Therapy. *Spectrochimica Acta A: Mol. Biomol. Spectrosc.* 250, 119363. doi:10.1016/j.saa.2020.119363
- Lopez-Salas, N., Kossmann, J., and Antonietti, M. (2020). Rediscovering Forgotten Members of the Graphene Family. *Acc. Mater. Res.* 1, 117–122. doi:10.1021/accountsmr.0c00011
- Ma, X., Li, L., Zeng, Z., Chen, R., Wang, C., Zhou, K., et al. (2019). Synthesis of Nitrogen-Rich Nanoporous Carbon Materials with C<sub>3</sub>N-type from ZIF-8 for Methanol Adsorption. *Chem. Eng. J.* 363, 49–56. doi:10.1016/j.cej.2019.01.132
- Mahmood, J., Lee, E. K., Jung, M., Shin, D., Choi, H.-J., Seo, J.-M., et al. (2016a). Two-dimensional Polyaniline (C<sub>3</sub>N) from Carbonized Organic Single Crystals in Solid State. *Proc. Natl. Acad. Sci.* 113 (27), 7414–7419. doi:10.1073/pnas.1605318113
- Mahmood, J., Lee, E. K., Jung, M., Shin, D., Choi, H.-J., Seo, J.-M., et al. (2016b). Two-dimensional Polyaniline (C<sub>3</sub>N) from Carbonized Organic Single Crystals in Solid State. *Proc. Natl. Acad. Sci. USA* 113, 7414–7419. doi:10.1073/pnas.1605318113
- Mahmood, J., Lee, E. K., Jung, M., Shin, D., Jeon, I.-Y., Jung, S.-M., et al. (2015). Nitrogenated Holey Two-Dimensional Structures. *Nat. Commun.* 6, 6486. doi:10.1038/ncomms7486
- Mane, G. P., Talapaneni, S. N., Lakhi, K. S., Ilbeygi, H., Ravon, U., Al-Bahily, K., et al. (2017). Highly Ordered Nitrogen-Rich Mesoporous Carbon Nitrides and Their Superior Performance for Sensing and Photocatalytic Hydrogen Generation. *Angew. Chem. Int. Ed.* 56, 8481–8485. doi:10.1002/anie.201702386
- Mazzanti, S., and Savateev, A. (2020). Emerging Concepts in Carbon Nitride Organic Photocatalysis. *ChemPlusChem* 85, 2499–2517. doi:10.1002/cplu.202000606
- Naseri, A., Samadi, M., Pourjavadi, A., Moshfegh, A. Z., and Ramakrishna, S. (2017). Graphitic Carbon Nitride (G-C<sub>3</sub>N<sub>4</sub>)-Based Photocatalysts for Solar Hydrogen Generation: Recent Advances and Future Development Directions. *J. Mater. Chem. A* 5, 23406–23433. doi:10.1039/c7ta05131j
- Nasir, M. S., Yang, G., Ayub, I., Wang, S., Wang, L., Wang, X., et al. (2019). Recent Development in Graphitic Carbon Nitride Based Photocatalysis for Hydrogen Generation. *Appl. Catal. B: Environ.* 257, 117855. doi:10.1016/j.apcatb.2019.117855
- Ning, X., and Lu, G. (2020). Photocorrosion Inhibition of CdS-Based Catalysts for Photocatalytic Overall Water Splitting. *Nanoscale* 12, 1213–1223. doi:10.1039/c9nr09183a
- Ong, W.-J., Tan, L.-L., Ng, Y. H., Yong, S.-T., and Chai, S.-P. (2016). Graphitic Carbon Nitride (G-C<sub>3</sub>N<sub>4</sub>)-Based Photocatalysts for Artificial Photosynthesis and Environmental Remediation: Are We a Step Closer to Achieving Sustainability. *Chem. Rev.* 116, 7159–7329. doi:10.1021/acs.chemrev.6b00075
- Qin, G., Cui, Q., Yun, B., Sun, L., Du, A., and Sun, Q. (2018). High Capacity and Reversible Hydrogen Storage on Two Dimensional C<sub>2</sub>N Monolayer Membrane. *Int. J. Hydrogen Energ.* 43, 9895–9901. doi:10.1016/j.ijhydene.2018.04.065
- Reischauer, S., and Pieber, B. (2021). Emerging Concepts in Photocatalytic Organic Synthesis. *iScience* 24, 102209. doi:10.1016/j.isci.2021.102209
- Savateev, A., Ghosh, I., König, B., and Antonietti, M. (2018). Photoredox Catalytic Organic Transformations Using Heterogeneous Carbon Nitrides. *Angew. Chem. Int. Ed.* 57, 15936–15947. doi:10.1002/anie.201802472
- Shi, L.-B., Zhang, Y.-Y., Xiu, X.-M., and Dong, H.-K. (2018). Structural Characteristics and Strain Behavior of Two-Dimensional C<sub>3</sub>N : First Principles Calculations. *Carbon* 134, 103–111. doi:10.1016/j.carbon.2018.03.076
- Shirazi, A. H. N., Abadi, R., Izadifar, M., Alajlan, N., and Rabczuk, T. (2018). Mechanical Responses of Pristine and Defective C<sub>3</sub>N Nanosheets Studied by Molecular Dynamics Simulations. *Comput. Mater. Sci.* 147, 316–321. doi:10.1016/j.commatsci.2018.01.058
- Singh, N. K., Pramoda, K., Gopalakrishnan, K., and Rao, C. N. R. (2018). Synthesis, Characterization, Surface Properties and Energy Device Characteristics of 2D Borocarbonitrides, (BN)<sub>x</sub>C<sub>1-x</sub>, Covalently Cross-Linked with Sheets of Other 2D Materials. *RSC Adv.* 8, 17237–17253. doi:10.1039/c8ra01885e
- Srinivasa, K., Modak, B., and Ghosh, S. K. (2014). Porous Graphitic Carbon Nitride: A Possible Metal-free Photocatalyst for Water Splitting. *J. Phys. Chem. C* 118, 26479–26484. doi:10.1021/jp506538d
- Tagani, M. B. (2018). Electrical and Mechanical Properties of a Fully Hydrogenated Two-Dimensional Polyaniline Sheet. *Comput. Mater. Sci.* 153, 126–133. doi:10.1016/j.commatsci.2018.06.027
- Tan, L., Nie, C., Ao, Z., Sun, H., An, T., and Wang, S. (2021). Novel Two-Dimensional Crystalline Carbon Nitrides beyond G-C<sub>3</sub>N<sub>4</sub>: Structure and Applications. *J. Mater. Chem. A* 9, 17–33. doi:10.1039/d0ta07437c
- Tian, Z., López-Salas, N., Liu, C., Liu, T., and Antonietti, M. (2020). C<sub>2</sub>N: A Class of Covalent Frameworks with Unique Properties. *Adv. Sci.* 7, 2001767. doi:10.1002/advs.202001767
- Vadivel, S., Hariganesh, S., Paul, B., Rajendran, S., Habibi-Yangjeh, A., Maruthamani, D., et al. (2020). Synthesis of Novel AgCl Loaded G-C<sub>3</sub>N<sub>5</sub> with Ultrahigh Activity as Visible Light Photocatalyst for Pollutants Degradation. *Chem. Phys. Lett.* 738, 136862. doi:10.1016/j.cplett.2019.136862
- Wang, H., Li, M., Lu, Q., Cen, Y., Zhang, Y., and Yao, S. (2019). A Mesoporous Rod-like G-C<sub>3</sub>N<sub>5</sub> Synthesized by Salt-Guided Strategy: As a Superior Photocatalyst for Degradation of Organic Pollutant. *ACS Sustain. Chem. Eng.* 7, 625–631. doi:10.1021/acssuschemeng.8b04182
- Wang, L., Wang, K., He, T., Zhao, Y., Song, H., and Wang, H. (2020a). Graphitic Carbon Nitride-Based Photocatalytic Materials: Preparation Strategy and Application. *ACS Sustain. Chem. Eng.* 8, 16048–16085. doi:10.1021/acssuschemeng.0c05246
- Wang, L., Zheng, X., Chen, L., Xiong, Y., and Xu, H. (2018a). Van der Waals Heterostructures Comprised of Ultrathin Polymer Nanosheets for Efficient Z-Scheme Overall Water Splitting. *Angew. Chem. Int. Ed.* 57, 3454–3458. doi:10.1002/anie.201710557
- Wang, X., Li, Q., Wang, H., Gao, Y., Hou, J., and Shao, J. (2018b). Anisotropic Carrier Mobility in Single- and Bi-layer C<sub>3</sub>N Sheets. *Physica B: Condensed Matter* 537, 314–319. doi:10.1016/j.physb.2018.02.015

- Wang, X., Maeda, K., Thomas, A., Takanabe, K., Xin, G., Carlsson, J. M., et al. (2009). A Metal-free Polymeric Photocatalyst for Hydrogen Production from Water under Visible Light. *Nat. Mater* 8, 76–80. doi:10.1038/nmat2317
- Wang, Z., Luo, Z., Li, J., Yang, K., and Zhou, G. (2020b). 2D van der Waals heterostructures of graphitic BCN as direct Z-scheme photocatalysts for overall water splitting: the role of polar  $\pi$ -conjugated moieties. *Phys. Chem. Chem. Phys.* 22, 23735–23742. doi:10.1039/d0cp04219f
- Wen, J., Xie, J., Chen, X., and Li, X. (2017). A Review on G-C 3 N 4 -based Photocatalysts. *Appl. Surf. Sci.* 391, 72–123. doi:10.1016/j.apsusc.2016.07.030
- Wu, Y., Xia, W., Gao, W., Jia, F., Zhang, P., and Ren, W. (2018). Quasiparticle Electronic Structure of Honeycomb C 3 N: from Monolayer to Bulk. *2d Mater.* 6, 015018. doi:10.1088/2053-1583/aaeaa
- Xu, J., Mahmood, J., Dou, Y., Dou, S., Li, F., Dai, L., et al. (2017). 2D Frameworks of C 2 N and C 3 N as New Anode Materials for Lithium-Ion Batteries. *Adv. Mater.* 29, 1702007. doi:10.1002/adma.201702007
- Yang, S., Li, W., Ye, C., Wang, G., Tian, H., Zhu, C., et al. (2017). C3 N-A 2D Crystalline, Hole-free, Tunable-Narrow-Bandgap Semiconductor with Ferromagnetic Properties. *Adv. Mater.* 29, 1605625. doi:10.1002/adma.201605625
- Yang, X., and Wang, D. (2018). Photocatalysis: From Fundamental Principles to Materials and Applications. *ACS Appl. Energ. Mater.* 1, 6657–6693. doi:10.1021/acsaem.8b01345
- Yin, H., Cao, Y., Fan, T., Zhang, M., Yao, J., Li, P., et al. (2021). *In Situ* synthesis of Ag3PO4/C3N5 Z-Scheme Heterojunctions with Enhanced Visible-Light-Responsive Photocatalytic Performance for Antibiotics Removal. *Sci. Total Environ.* 754, 141926. doi:10.1016/j.scitotenv.2020.141926
- Yin, H., Guo, Q., He, D., Li, J., and Sun, S. (2017). Structural Characterization and Electrochemical Performance of Macroporous Graphite-like C3N3 Prepared by the Wurtz Reaction and Heat Treatment. *RSC Adv.* 7, 44001–44008. doi:10.1039/c7ra07707f
- Yuan, T., Zheng, M., Antonietti, M., and Wang, X. (2021). Ceramic boron Carbonitrides for Unlocking Organic Halides with Visible Light. *Chem. Sci.* 12, 6323–6332. doi:10.1039/d1sc01028j
- Zeng, J., Chen, Z., Zhao, X., Yu, W., Wu, S., Lu, J., et al. (2019). From All-Triazine C3N3 Framework to Nitrogen-Doped Carbon Nanotubes: Efficient and Durable Trifunctional Electrocatalysts. *ACS Appl. Nano Mater.* 2, 7969–7977. doi:10.1021/acsnm.9b02011
- Zhang, C., Jiao, Y., He, T., Bottle, S., Frauenheim, T., and Du, A. (2018). Predicting Two-Dimensional C3B/C3N van der Waals p-n Heterojunction with Strong Interlayer Electron Coupling and Enhanced Photocurrent. *J. Phys. Chem. Lett.* 9, 858–862. doi:10.1021/acs.jpcclett.7b03449
- Zhang, J., Tao, H., Wu, S., Yang, J., and Zhu, M. (2021). Enhanced Durability of Nitric Oxide Removal on TiO2 (P25) under Visible Light: Enabled by the Direct Z-Scheme Mechanism and Enhanced Structure Defects through Coupling with C3N5. *Appl. Catal. B: Environ.* 296, 120372. doi:10.1016/j.apcatb.2021.120372
- Zhang, X., Luo, X., Zheng, X., Wu, X., and Xu, H. (2019). Protonation-Assisted Exfoliation of N-Containing 2D Conjugated Polymers. *Small* 15, e1903643. doi:10.1002/smll.201903643
- Zhou, L., Zhang, H., Sun, H., Liu, S., Tade, M. O., Wang, S., et al. (2016). Recent Advances in Non-metal Modification of Graphitic Carbon Nitride for Photocatalysis: A Historic Review. *Catal. Sci. Technol.* 6, 7002–7023. doi:10.1039/c6cy01195k
- Zou, Y., Xiao, K., Qin, Q., Shi, J.-W., Heil, T., Markushyna, Y., et al. (2021). Enhanced Organic Photocatalysis in Confined Flow through a Carbon Nitride Nanotube Membrane with Conversions in the Millisecond Regime. *ACS Nano* 15, 6551–6561. doi:10.1021/acsnano.0c09661

**Conflict of Interest:** The authors declare that the research was conducted in the absence of any commercial or financial relationships that could be construed as a potential conflict of interest.

**Publisher's Note:** All claims expressed in this article are solely those of the authors and do not necessarily represent those of their affiliated organizations, or those of the publisher, the editors, and the reviewers. Any product that may be evaluated in this article, or claim that may be made by its manufacturer, is not guaranteed or endorsed by the publisher.

Copyright © 2021 López-Salas and Albero. This is an open-access article distributed under the terms of the Creative Commons Attribution License (CC BY). The use, distribution or reproduction in other forums is permitted, provided the original author(s) and the copyright owner(s) are credited and that the original publication in this journal is cited, in accordance with accepted academic practice. No use, distribution or reproduction is permitted which does not comply with these terms.